Nano Energy 73 (2020) 104801

Contents lists available at ScienceDirect

Nano Energy

journal homepage: http://www.elsevier.com/locate/nanoen

Designed growth and patterning of perovskite nanowires for lasing and wide color gamut phosphors with long-term stability

Chun-Ho Lin [a,d], Ting-You Li [a], Jing Zhang [a], Zong-Yi Chiao [b,c], Pai-Chun Wei [a], Hui-Chun Fu [a], Long Hu [d], Meng-Ju Yu [b,c], Ghada H. Ahmed [e], Xinwei Guan [d], Chih-Hsiang Ho [f], Tom Wu [d], Boon S. Ooi [a], Omar F. Mohammed [e], Yu-Jung Lu [b,c], Xiaosheng Fang [g,**], Jr-Hau He [a,h,*]

[a] Computer, Electrical, and Mathematical Sciences and Engineering Division, King Abdullah University of Science and Technology (KAUST), Thuwal, 23955-6900, Saudi Arabia
[b] Research Center for Applied Sciences, Academia Sinica, Taipei, 11529, Taiwan, ROC
[c] Department of Physics, National Taiwan University, Taipei, 10617, Taiwan, ROC
[d] School of Materials Science and Engineering, University of New South Wales (UNSW), Sydney, NSW, 2052, Australia
[e] Division of Physical Science and Engineering, King Abdullah University of Science and Technology (KAUST), Thuwal, 23955-6900, Saudi Arabia
[f] Raysolution LLC, San Jose, CA, 95129, USA
[g] Department of Materials Science. Fudan University, Shanghai, 200433, PR China
[h] Department of Materials Science and Engineering, City University of Hong Kong, Kowloon, Hong Kong

ARTICLE INFO

Keywords:
Perovskite
Nanowire
Patterning
Printing
Stability

ABSTRACT

Hybrid halide perovskites are proposed for next-generation photovoltaics and lighting technologies due to their remarkable optoelectronic properties. In this study, we demonstrate printed perovskite nanowires (NWs) for lasing and wide-gamut phosphor using a combination of inkjet printing and nanoporous anodic aluminum oxide (AAO). The random lasing behaviors of the resulting perovskite NWs are analyzed and discussed. Moreover, by varying the composition of Cl^-, Br^-, and I^- anions, we demonstrate tunable emission wavelengths of the perovskite NWs from 439 to 760 nm, with a large red-green-blue color space that extends to 117% of the color standard defined by the National Television Systems Committee (NTSC). Furthermore, we demonstrate passivation of the perovskite NWs against moisture due to their compact spatial confinement within the AAO template combined with a poly(methyl methacrylate) sealing process, resulting in highly stable emission intensity that degrades only 19% after continuous 250 h of 30 mW/cm^2 UV excitation and degrades 30% after three months when stored in air at 50% humidity. This inkjet printing fabrication strategy involving AAO-confined perovskite NWs enables highly stable, large-area direct patterning and mass production of perovskite NWs, which is promising for modern lighting applications.

1. Introduction

Organic-inorganic halide perovskites ($MAPbX_3$, $MA = CH_3NH_3^+$; $X = Cl^-$, Br^- or I^-), possessing the same crystal structure as mineral $CaTiO_3$, have incredible potential for optoelectronic applications due to their superior light-absorption, long charge carrier diffusion lengths, high carrier mobility, slow rates of non-radiative charge recombination, and intense photoluminescence (PL) [1–6]. In recent years, perovskite optoelectronics have advanced by leaps and bounds for both light harvesting (solar cells and photodetectors) [7–10] and light emitting devices (light emitting diodes (LEDs) and lasers) [11–14] using various perovskite structures and designs. Among nanostructured perovskites, one-dimensional perovskite nanowires (NWs) have demonstrated great potential for lighting applications compared to bulk perovskites as a result of their small size, one-dimensionally confined excitons, and efficient photon coupling, as well as serving as excellent waveguides and natural cavities [15–20]. For example, Zhu et al. have reported a surface-initiated solution grown perovskite NW laser with an extremely high lasing quality factor (Q) of 3600, which shows the potential of this material for advanced lighting devices [12]. Although tremendous

* Corresponding author. Computer, Electrical, and Mathematical Sciences and Engineering Division, King Abdullah University of Science and Technology (KAUST), Thuwal, 23955-6900, Saudi Arabia.
** Corresponding author.
E-mail addresses: xshfang@fudan.edu.cn (X. Fang), jrhauhe@cityu.edu.hk (J.-H. He).

https://doi.org/10.1016/j.nanoen.2020.104801
Received 1 February 2020; Received in revised form 25 March 2020; Accepted 2 April 2020
Available online 17 April 2020

success has been demonstrated using perovskite NWs in nanophotonics, it remains challenging to pattern, align, and transfer these materials for large-scale lighting applications.

The poor stability of perovskites is another crucial obstacle for commercial applications [21,22]. Due to their ionic nature, halide perovskites are sensitive to highly polar compounds (*e.g.*, moisture and oxygen) and readily degrade in air [23]. As a result, a variety of strategies have been proposed to enhance the stability of perovskite devices, such as the substitution of MA and Pb with other cations [24,25], the addition of diffusion blocking layers [26] and ion migration-retarding additives [27], as well as Ruddlesden–Popper phase [28] and Dion–Jacobson phase [29] engineering. In 2017, Grancini et al. reported a perovskite solar cell that displayed stable performance for over a year, which was made possible by interface engineering [30]. However, the operational lifetimes of most perovskite-based LEDs, lasers, and other lighting devices are still less than 100 h due to the large amounts of heat and energy that are generated during light emission [31–34]. Recently, nanostructure-template confined growth has been demonstrated as an effective method of improving the long-term stability of perovskites by (i) providing protection against moisture via the surrounding nanostructural-template and (ii) restricting the expansion of the perovskite, which is required in the phase transition of the material when exposed to moisture and oxygen, thus mitigating the degradation reaction [35,36]. Using this technique, several groups have reported perovskite devices that remain stable for months, even while stored in atmosphere [36–38].

In this study, we introduce an inkjet printing method to fabricate and pattern perovskite NW arrays within nanoporous anodic aluminum oxide (AAO), which acts as a nanostructured template to confine the perovskite growth into the NW shape (Fig. 1) while simultaneously improving the material's stability. Printing is a high quality, simple, inexpensive, and rapid fabrication process that can enable the mass production of microelectronic devices. With this strategy, we demonstrate printed perovskite NWs that feature random lasing capability at a threshold pump fluence of 140 mJ cm^{-2} and a Q factor of 150. Additionally, by varying the composition of the halide anions (Cl^-, Br^-, and I^-), we can tune the PL of the perovskite NWs from 439 to 760 nm, with the resulting red-green-blue (RGB) CIE coordinates covering a larger color space (117%) than the standard defined by the National Television Systems Committee (NTSC). We also grind the AAO-confined perovskite NWs into powders to demonstrate the material for phosphor applications. To verify the stability of this printed material, we show that the passivation effect provided by the compact spatial confinement of the AAO combined with a poly(methyl methacrylate) (PMMA) sealing process results in a high operational lifetime of 250 h (19% degradation) under 30 mW/cm^2 UV illumination and a long-term stability of over 3 months (30% degradation) under indoor lighting in air with 50% humidity. Furthermore, this large-scale fabrication method using inkjet printing allows flexible patterning of the perovskite NWs, avoiding the need for additional transfer processes. The strategy described herein provides a new way to mass-produce high-quality perovskite NWs for wide color gamut and large-scale lighting applications.

2. Results and discussion

2.1. Fabrication and characterization of printed perovskite NWs

We first synthesized $CH_3NH_3PbBr_3$ perovskite NWs using an inkjet printing process shown in Fig. 1 (see Experimental Section for details). First, the perovskite inks were prepared by dissolving the perovskite precursors in dimethylformamide (DMF). Then, we inkjet-printed these perovskite solutions on a nanoporous AAO substrate. During the printing process, vacuum pumping was applied to the back side of the AAO substrate to guide the perovskite inks into the nanopores, confining the perovskite growth into NW shapes templated by the AAO pores. Finally, the sample was annealed at 90 °C on a hotplate for 2 h to remove the DMF solvent and improve the crystalline quality of the perovskite.

This fabrication method incorporating inkjet printing and nanopore-confined growth enables flexible patterning with precise alignment for large-scale lighting applications. The drop size of our inkjet printer is ~60 μm while the contact angle between perovskite inks and AAO is 49.7° (Fig. S1). Under this circumstance, the printing resolution is limited to ~100 μm. Fig. 2a demonstrates PL images of the printed perovskites within the template under UV illumination, demonstrating the different patterns that can be achieved on the AAO substrate by inkjet printing. Other fabrication methods, such as chemical vapor deposition and capillary growth, are also compatible with AAO but lack the capability to design flexible patterns [39–41]. Using inkjet printing, the realization of patterning opens a variety of possibilities of using perovskite NW arrays as phosphors, sensors, photonic crystals, nanolasers, and biosensors with controlled density, location, feature size, and distribution according to the desired device requirements.

Fig. S2a shows a top-view scanning electron microscopy (SEM) image of the border between the printed and unprinted regions of the AAO substrate, in which the surface morphologies clearly show the $CH_3NH_3PbBr_3$ perovskite material covering the surface of the printed AAO. Fig. S2b displays high-resolution top-view SEM images revealing the empty nanopores of the unprinted AAO region, while the printed nanopores are filled with perovskite. We conducted cross-sectional SEM characterization to verify the presence of the perovskite NWs in the AAO nanopores (Fig. 2b). The thickness of the AAO substrate was 50 μm. Our results showed that the effective diffusion depth of the perovskite inks was about 5–10 μm, with most of the perovskite NWs distributed in the upper region of the AAO substrate. The cross-sectional PL mapping in Fig. 2c reveals intense PL in the upper region of the substrate with a thickness of around 5–10 μm, which is in good agreement with the SEM measured distribution of the perovskite NWs in the AAO nanopores. Fig. S3a also shows a high-resolution cross-sectional SEM image, which clearly indicates the presence of perovskite NWs within the AAO nanopores. The lengths of the perovskite NWs vary from a few μm to 10 μm and the diameters range from dozens of nm to 200 nm. Generally, perovskite NWs with short diameter should exhibit better fluorescence

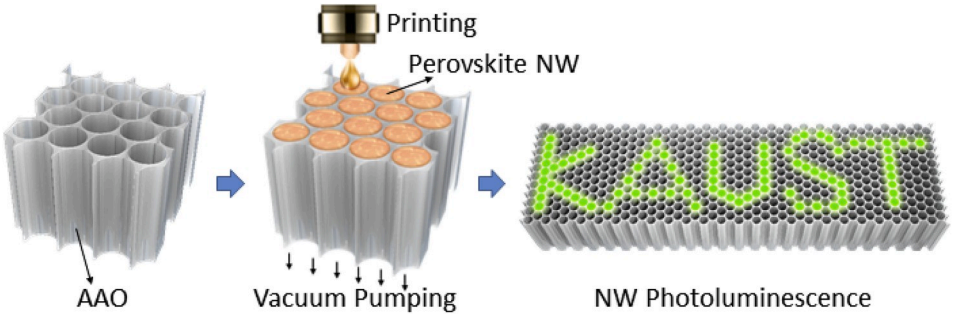

Fig. 1. Schematic of the fabrication process for printing perovskite NWs in the nanoporous AAO for lighting applications.

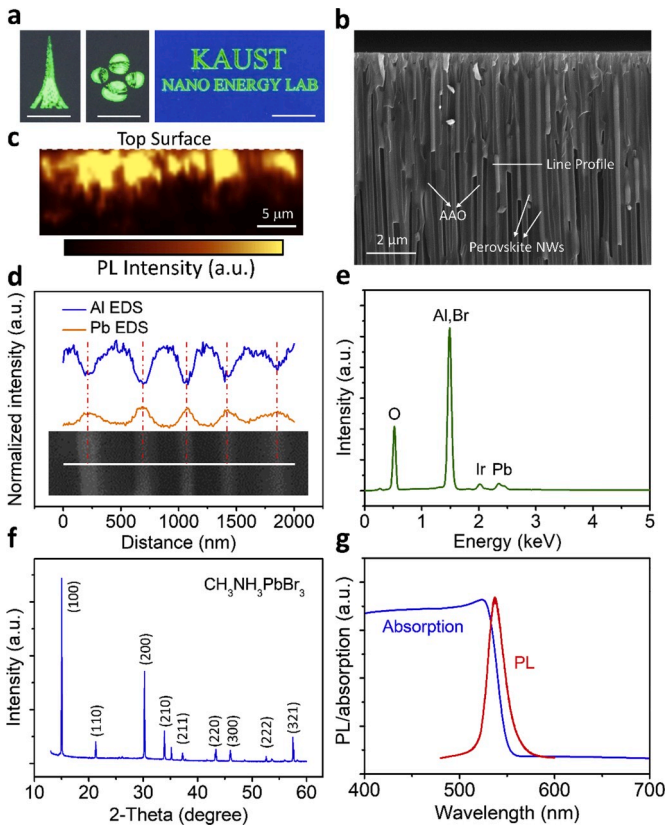

Fig. 2. Characterization of the printed $CH_3NH_3PbBr_3$ perovskite NWs templated in AAO nanopores. (a) Optical images of the printed perovskite NWs with different patterns under UV illumination. The scale bars are 5 mm. (b) Cross-sectional SEM image of the perovskite NWs in the AAO nanopores. (c) Cross-sectional PL mapping of the perovskite NWs. (d) SEM/EDS line scan analysis along the line profile of Fig. 2b. (e) EDS spectrum of the perovskite NWs in the AAO nanostructure. (f) XRD pattern of the perovskite NWs. (g) The PL (excitation wavelength = 473 nm) and absorption spectra of the perovskite NWs.

performance due to strong quantum confinement. We note that the diameters of studied perovskite NWs are larger than the Bohr radius [42], however, these structures do feature center-of-mass confinement, which can still provide a good quantum effect in the NW structure [43,44]. It is worth noting that the commercial AAO has a narrow pore entrance layer at the top with a diameter of about 20 nm (Figs. S2b and S3b). Therefore, the diameters of the porous entrance and perovskite NWs are distinct.

The compositions of the perovskite NWs and AAO were confirmed by energy dispersive spectroscopy (EDS) line scan analysis, as shown in Fig. 2d, in which the perovskite NWs reveal Pb signals while the AAO template features Al content (the EDS spectrum is shown in Fig. 2e). We then characterized the $CH_3NH_3PbBr_3$ NWs by X-ray diffraction (XRD), ultraviolet–visible (UV–Vis), and PL spectroscopies. The XRD spectrum in Fig. 2f shows sharp and strong peaks that agree with previous reports of $CH_3NH_3PbBr_3$ perovskite [45], illustrating the high purity of the NWs. Furthermore, the UV–Vis optical absorption spectrum is shown in Fig. 2g, which reveals a band edge cut-off that corresponds to the material's PL peak emission of 536 nm (energy equal to a bandgap of 2.31 eV).

2.2. Lasing behavior of perovskite NWs

We studied the lasing behavior of the $CH_3NH_3PbBr_3$ NWs at a temperature of 4.5 K. A regeneratively amplified femtosecond Ti:sapphire laser was used to optically pump the sample using 84-fs, 400-nm pulses at a repetition rate of 1 kHz. Fig. 3a shows the emission spectra of the $CH_3NH_3PbBr_3$ NWs at different optical pump fluences. When the NWs is pumped with low fluence of 5 mJ cm^{-2}, below the lasing threshold, a broad spontaneous emission spectrum can be obtained with a full width at half maximum (FWHM) of 11 nm. As the pump fluence increases above the lasing threshold, for example, at 1.3 J cm^{-2}, a sharp stimulated lasing emerges with a narrow FWHM of 3.5 nm [46]. Fig. 3b illustrates the integrated emission intensity and FWHM as a function of the pump fluence, which follows the typical S-shape lasing curve. The S-curve indicates the integrated emission transitions from the SE mode to stimulated lasing [47] as the excitation fluence rises above the lasing threshold of 140 mJ cm^{-2}. At the same time, the FWHM plot shows a sudden drop at the lasing threshold and becomes constant at around 3.5 nm in the stimulated lasing mode. Because there is a narrow pore entrance layer of AAO with a thickness of ~200 nm at the top of perovskite NWs, as shown in the cross-sectional SEM image in Figs. S3b and a high lasing threshold of 140 mJ cm^{-2} is needed to effectively excite the perovskite NWs below the AAO narrow entrance layer. Using AAO without narrow entrance layer would significantly reduce the threshold, which can be achieved by lithography fabrication of highly ordered AAO [48]. The decrease of exciton lifetime is an important feature for lasing [10]. Fig. 3c illustrates the time-resolved PL decay for SE and lasing of the perovskite NWs. The apparent SE lifetime (τ_{SE}) was obtained as ~4 ns, while the lasing lifetime (τ_{lasing}) reduced to ≤100 ps dramatically, thus verifying the occurrence of lasing. To emphasize the difference between SE and lasing, the normalized spectra of the two emission modes are shown in Fig. 3d, which confirms the much sharper peak emission of the lasing mode.

For traditional Fabry-Perot, whispering gallery mode, and photonic crystal lasers, a structured cavity is required to emit coherent lasing light [49,50]. However, the varied dimensions of the perovskite NWs within the highly disordered AAO nanopores (Figs. S2b and S3) suggest that traditional lasing modes are unlikely to occur due to the lack of a well-defined cavity. We speculate that the lasing behaviors we observed in the perovskite NWs are caused by mirrorless random lasing because the nanostructures are highly disordered. Furthermore, several groups have reported random lasing based on similar randomly-distributed nanopores [49,51]. Random lasing was generated by strong multiple light scattering in random gain perovskite NW media without the need for a high-quality cavity [52]. In our study, since the spot size of the pumping laser is 1 μm in diameter, we can only obtain the lasing signals

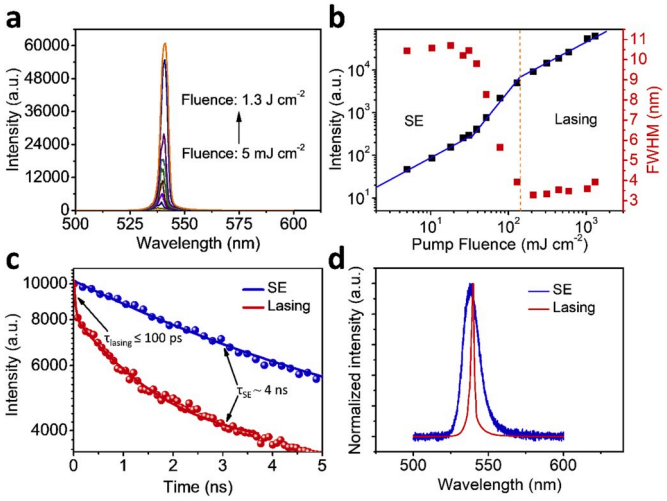

Fig. 3. SE and lasing characterization of the printed $CH_3NH_3PbBr_3$ perovskite NWs. (a) Emission spectra of the NWs at different optical pump fluences, ranging from 5 mJ cm^{-2} to 1.3 J cm^{-2}. (b) Integrated emission intensity and FWHM as a function of the pump fluence of the printed $CH_3NH_3PbBr_3$ perovskite NWs. (c) Time-resolved PL decay for SE and lasing of the NWs. (d) SE and lasing spectra of the printed $CH_3NH_3PbBr_3$ perovskite NWs.

from many NWs. It should be noted that in the green wavelength around 536 nm, the transmittance of AAO is larger than 75% (Fig. S4), which means the green emission can easily penetrate through thin AAO wall and interact with neighboring perovskite NWs, resulting in random scattering cavity. The lasing Q factor (defined as λ/FWHM) of the $CH_3NH_3PbBr_3$ NWs was around 150, which is comparable with other perovskite based random lasing studies as shown in Table S1 [53–58]. Because the dimensions of the printed perovskite NWs vary with the nonuniform nanopore diameters of the AAO substrate, the light scattering in the individual NWs can vary from each other. Moreover, since the lasing signals were obtained from many NWs, a slightly wide FWHM of 3.5 nm was observed, which leads to a low lasing Q factor. Therefore, using an AAO substrate with more uniform nanopore sizes may help improve the Q factor of the perovskite NW laser.

2.3. Printed perovskite NWs for wide color gamut phosphors

Another important advantage of our AAO structural design is that the PL of the perovskite can be significantly amplified by the nanoporous confinement. To understand the effect of the substrate, we ran a control experiment in which the perovskite inks were printed on either AAO or a flat Al_2O_3 substrate, which possesses the same composition as the AAO but without the porous nanostructures. We found that the perovskite with AAO substrate can emit bright green light under UV illumination, while the emission of perovskite with flat Al_2O_3 substrate was too weak to be observed under the same UV condition (Fig. S5a). The PL spectra of two samples were also obtained as shown in Fig. S5b. For the AAO specimen, we observed strong PL with an emission intensity an order of magnitude larger than the sample printed on the flat Al_2O_3 substrate, demonstrating the superiority of the nanoporous design. This result can be attributed to the better NW crystal growth and center-of-mass confinement in the nanoporous AAO, which increases the radiative carrier recombination and leads to the significantly amplified PL emission. The quantum yield of perovskite NWs within the AAO were obtained to be 30%, which is comparable with perovskite NWs and nanorods in other reports as shown in Table S2 [59–63].

Due to the intense PL emission, a suitable application for these perovskite NWs is as phosphors, which are substances that exhibit strong PL and are commonly used in sensors, fluorescent lights, white LEDs, and display technology. To meet the demand for colorful phosphors, we demonstrate that the PL properties of the NWs can be tuned by varying the anion elemental composition of the perovskite. Fig. 4a shows the composition-dependent PL spectra of the $CH_3NH_3PbX_3$ NWs with peak wavelengths tuned from 439 nm to 736 nm. The $CH_3NH_3PbBr_3$ NWs emit bright green light with a wavelength of 536 nm under UV illumination. When Cl^- ions are added to the perovskite inks, the printed $CH_3NH_3Pb(Cl_{1-x}Br_x)_3$ NWs demonstrated blue-shifted PL as the concentration of Cl^- was increased. In contrast, we observed red-shifted PL when I^- ions were introduced. Additionally, it is found that the $CH_3NH_3PbBr_xI_{3-x}$ possesses a much broader emission peak at 646 nm, indicating that the phase segregation may occur between Br^- and I^- ions [64]. The corresponding optical images of the $CH_3NH_3PbX_3$ NWs with different composition of the halide anions are shown in Fig. 4b, which illustrates eight different colors of emission under UV excitation.

RGB perovskite NWs are the most vital materials for the application in wide color gamut phosphors. Fig. 4c displays the CIE coordinates of red $CH_3NH_3PbI_3$ (0.67, 0.31), green $CH_3NH_3PbBr_3$ (0.14, 0.76), and blue $CH_3NH_3PbCl_3$ (0.16, 0.04) perovskite NWs measured using a spectrometer. A comparison of RGB peak position and the FWHM with perovskite NWs in other reports is also shown in Table S3 [65–69]. To further analyze the RGB colors, we used the NTSC system, which is a key parameter for determining the color space of phosphors. Using the equation $\text{NTSC}\ (\%) = (R_xG_y + R_yB_x + G_xB_y - R_xB_y - G_xR_y - B_xG_y) \div 0.3164$, we calculated the RGB color gamut area of our perovskite NWs to be approximately 117% of the NTSC. The large NTSC value demonstrated here confirms the ability of the inkjet-printed

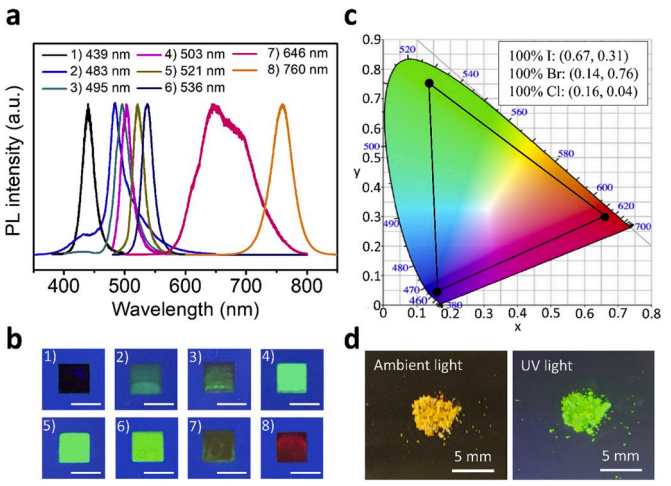

Fig. 4. Color-tunable PL of the perovskite NWs. (a) Composition-dependent PL emission spectra of perovskite NWs. The composition of 8 different perovskite NWs is shown in the Experimental Section. (b) The optical images of the perovskite NWs with 8 different colors under UV illumination. The scale bars are 3 mm. (c) CIE diagram showing the RGB coordinates of the perovskite NWs (sample number 1, 6, and 8 in Fig. 4b). (d) Photographs of the perovskite NW phosphor powders under ambient light and UV illumination.

perovskite NWs to serve in wide color gamut applications, such as display screens, fluorescent lights, and white light sources. Additionally, because of its nanoporous structure and material nature, the AAO substrate is brittle and thus easy to grind into powder. Fig. 4d shows photos of a $CH_3NH_3PbBr_3$ perovskite NW powder sample under ambient light and UV illumination, in which the bright green light emission under UV excitation confirms the material's capability to be utilized as a phosphor powder. It would be convenient to coat such perovskite NW phosphor powders on objects with different shapes and curvilinear surfaces, thus enabling extensive phosphor lighting applications.

2.4. Stability of printed perovskite NWs

Stability is a particularly important characteristic of moisture-sensitive perovskites. Herein, we performed a stability test using four kinds of samples: (i) inkjet-printed $CH_3NH_3PbBr_3$ perovskite on a flat Al_2O_3 substrate; (ii) inkjet-printed $CH_3NH_3PbBr_3$ perovskite on a flat Al_2O_3 substrate with PMMA sealing; (iii) inkjet-printed AAO-confined perovskite NWs; and (iv) inkjet-printed AAO-confined perovskite NWs with PMMA sealing (see Experimental Section). Fig. 5a shows the excitation durability test, in which the peak PL intensities of the samples were measured under continuous 30 mW/cm^2 UV irradiation for up to 250 h in air with 50% average humidity. We can see that the perovskite

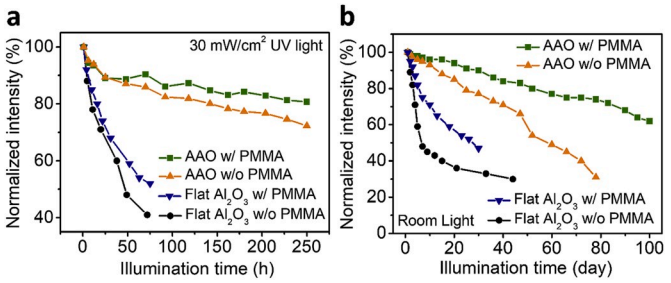

Fig. 5. Stability tests of perovskite-Al_2O_3, PMMA-sealed perovskite-Al_2O_3, perovskite-AAO, and PMMA-sealed perovskite-AAO. (a) Time-dependent PL intensity as the perovskite samples were exposed to continuous 30 mW/cm^2 UV excitation in air (50% humidity). (b) Time-dependent PL intensity of the perovskite samples under room lighting and 50% humidity in air.

NWs in the AAO substrate feature much lower deterioration than the perovskite on the flat Al_2O_3 substrate after this period of time, demonstrating the remarkable stability of the nanoporous AAO confinement design. Moreover, the operational durability can be further improved using PMMA sealing, and the printed perovskite NWs demonstrates only 19% deterioration after 250 h of continuous UV irradiation. Similar results were observed in the long-term stability test when the samples were stored under room lighting in air with 50% average humidity (Fig. 5b). The peak PL intensity of the perovskite on the flat Al_2O_3 substrate with PMMA sealing decreased by 50% after 25 days, whereas the perovskite NWs in AAO deteriorated by 50% after 60 days, and the PMMA-sealed perovskite NWs retained 70% of its PL intensity after 100 days. The stability of PMMA-sealed perovskite NWs were also tested under high humidity and temperature as shown in Fig. S6. The perovskite NWs retained 90% and 74% PL intensity after 1 month under 50% and 80% humidity, respectively. In addition, the perovskite NWs can alive for 4 days long under continuous heating at 100 °C.

The improved stability of the perovskite NWs can be attributed to the strong nanoporous confinement of the AAO [70]. The compact spatial confinement by the inert AAO provides a natural barrier against the moisture and oxygen in air. Moreover, previous research has reported that the hydrated perovskite phases $CH_3NH_3PbX_3 \bullet H_2O$ and $(CH_3NH_3)_4PbX_6 \bullet 2H_2O$ are formed in the initial degradation step [71,72]. These phase transitions involve the expansion of the perovskite crystal [36,73]. However, for perovskite NWs in the AAO nanopores, the expansion is prohibited due to the spatial confinement, which results in the suppression of the perovskite phase transition and thus improved stability. In addition to the nanoporous confinement, because the long-chain PMMA possesses low polarity and is chemically orthogonal to the perovskites [19], the use of PMMA sealing can further enhance the passivation to moisture.

3. Conclusion

In summary, we have fabricated perovskite NWs using inkjet printing and an AAO confinement strategy. The realization of a variety of NW patterns, featuring PL properties and center-of-mass amplified luminance, demonstrates the ability of this technique to fabricate complex electronic device designs with controlled density, location, diameter, and distribution of perovskite NWs. The perovskite NWs feature random lasing capability, with a lasing threshold of 140 mJ cm^{-2} and a Q factor of 150. Furthermore, wide-gamut emissions (439–760 nm) were achieved by varying the composition of the Cl^-, Br^-, and I^- anions in the perovskite, resulting in a large RGB color space of 117% of the NTSC standard. Additionally, we demonstrated phosphor powders made from the perovskite NWs, which can be readily adapted to different surfaces, thus enabling extensive wide color gamut phosphor applications. Because the AAO nanoporous confinement can suppress the perovskite phase transitions by restricting the expansion during the phase changes, we were able to demonstrate improved moisture stability in combination with PMMA sealing for a long lifetime of 250 h with just 19% PL degradation under 30 mW/cm^2 UV illumination along with a remarkable long-term stability of 100 days in air (50% humidity) with only 30% PL degradation. The scalable patterning and excellent alignment of this inkjet printing and AAO spatial confinement technique enabled us to synthesize perovskite NWs with valuable optical properties and high operational durability and long-term stability, suggesting a bright future of these low-cost fabricated materials in next-generation optoelectronics.

4. Experimental Section

4.1. Fabrication of printed perovskite NWs

To prepare the perovskite inks, an equimolar amount of $PbBr_2$ (99%, Sigma) and CH_3NH_3Br (98% Sigma) powders were dissolved in DMF solution with a molar concentration of 0.5 M each. The mixed solution was stirred on a hotplate at 90 °C for 24 h to make the perovskite inks. Finally, the inks were filtered through a 0.25 μm filter for printing purposes. A Fujifilm Dimatix inkjet printer (DMP-2831) was used to print the perovskite inks on the AAO substrate (Whatman, pore size 0.02 μm). During the printing process, a vacuum pump was employed on the bottom of the AAO substrate to guide the perovskite inks into the nanopores. Then, the sample was annealed at 90 °C for 2 h to obtain the perovskite NWs in the AAO nanopores.

4.2. Perovskite NW characterization

Top view and cross-sectional SEM images of the perovskite NW samples were taken using a Magellan™ XHR SEM with an accelerating voltage of 5 kV. 5-nm-thick Ir was coated on the sample to avoid charging effects during SEM examination. The phase purity of the perovskite NWs were surveyed by XRD using a Bruker D8 Advance diffractometer equipped with a Cu Ka X-ray tube. The contact angle between perovskite inks and AAO was measured using a DSA100 drop shape analyzer (KRÜSS GmbH). A Shimadzu UV 3600 spectrophotometer was used to investigate the optical absorption spectrum of the perovskite NWs. The PL spectra of the perovskite NWs were obtained through a fluorescence microscope system (NTEGRA Spectra, NT-MDT) with a 473-nm laser. The time-resolved photoluminescence measurement was carried out using a fluorescent spectrophotometer (HORIBA, Nanolog model), applying an excitation wavelength of 372 nm. The quantum yield of perovskite NWs was examined using a Jobin Yvon-Spex fluorolog-3 spectrometer. To study the chromatics of the $CH_3NH_3PbI_3$, $CH_3NH_3PbBr_3$, and $CH_3NH_3PbCl_3$ perovskite NWs, a GL-spectis spectrometer (GL Optic) was utilized to measure their RGB CIE coordinates. A UV box (UV2020-2, TOPBIO CO.) was used as the UV light source (30 mW/cm^2) in this study. Except for the experiments of the wide color gamut study in Fig. 4, all the data was obtained based on the $CH_3NH_3PbBr_3$ perovskite.

4.3. Lasing characterization

The lasing measurements were taken on a closed-cycle cryogenic system (Attodry 800, Attocube) at a temperature of 4.5 K equipped with a scanning confocal microscope and a spectrometer (Andor) consisting of a monochromator and a thermo-electric cooled CCD camera. A regeneratively amplified femtosecond Ti:sapphire laser (TOPAS, Spectra-Physics), providing 84-fs, 400-nm pulses at a repetition rate of 1 kHz, was used to optically pump the sample. A 100x objective lens (0.82 NA; Attocube) was used to focus the pulsed laser to a small spot of 1 μm in diameter. To filter out the excitation laser signal, a 420 nm long pass filter was placed before the spectrometer.

4.4. Growth of different perovskite NWs for wide color gamut applications

The wide color gamut behavior of the perovskite NWs was achieved by varying the composition of Cl^-, Br^-, and I^- anions. We prepared 8 different perovskite inks and followed the same fabrication process described in *4.1 Fabrication of printed perovskite NWs* to grow these perovskite NW samples. The composition of halide anions for the different inks is listed as follows: (1) 100% Cl; (2) 60% Cl + 40% Br; (3) 50% Cl + 50% Br; (4) 40% Cl + 60% Br; (5) 20% Cl + 80% Br; (6) 100% Br; (7) 10% I + 90% Br; and (8) 100% I.

4.5. PMMA sealing

The printed AAO substrate was first fixed on glass. 950 PMMA (A4) was spin-coated on the perovskite sample at 1500 rpm for 30 s, followed by baking at 90 °C for 2 h. Then, this PMMA coating process was repeated again to ensure the sealing of the perovskite NWs.

Declaration of competing interest

The authors declare no competing interests.

Acknowledgements

This work was financially supported by the King Abdullah University of Science and Technology (KAUST) Office of Sponsored Research (OSR) (OSR-2016-CRG5-3005), KAUST baseline funding, the Ministry of Science and Technology, Taiwan (Grant No. MOST-106-2112-M-001-036-MY3), Academia Sinica (Grant No. AS-CDA-108-M08), Australian Research Council (DP190103316), and the startup funding of City University of Hong Kong.

Appendix A. Supplementary data

Supplementary data to this article can be found online at https://doi.org/10.1016/j.nanoen.2020.104801.

References

[1] S.D. Stranks, H.J. Snaith, Nat. Nanotechnol. 10 (2015) 391–402.
[2] Q. Zhang, M.M. Tavakoli, L.L. Gu, D.Q. Zhang, L. Tang, Y. Gao, J. Guo, Y.J. Lin, S. F. Leung, S. Poddar, Y. Fu, Z.Y. Fan, Nat. Commun. 10 (2019) 727.
[3] C.Y. Kang, C.H. Lin, C.H. Lin, T.Y. Li, S.W. Huang Chen, C.L. Tsai, C.W. Sher, T. Z. Wu, P.T. Lee, X. Xu, M. Zhang, C.H. Ho, J.H. He, H.C. Kuo, Adv. Sci. 6 (2019) 1902230.
[4] N.J. Jeon, J.H. Noh, W.S. Yang, Y.C. Kim, S. Ryu, J. Seo, S.I. Seok, Nature 517 (2015) 476–480.
[5] Y. Fu, H. Zhu, J. Chen, M.P. Hautzinger, X.-Y. Zhu, S. Jin, Nat. Rev. Mater. 4 (2019) 169–188.
[6] Z. Liu, L. You, N. Faraji, C.H. Lin, X. Xu, J.H. He, J. Seidel, J. Wang, H.N. Alshareef, T. Wu, Adv. Funct. Mater. (2020) 1909672.
[7] W.Y. Nie, H.H. Tsai, R. Asadpour, J.C. Blancon, A.J. Neukirch, G. Gupta, J. J. Crochet, M. Chhowalla, S. Tretiak, M.A. Alam, H.L. Wang, A.D. Mohite, Science 347 (2015) 522–525.
[8] L.T. Dou, Y. Yang, J.B. You, Z.R. Hong, W.H. Chang, G. Li, Y. Yang, Nat. Commun. 5 (2014) 5404.
[9] A.M. Alamri, S. Leung, M. Vaseem, A. Shamim, J.H. He, IEEE Trans. Electron. Dev. 66 (2019) 2657–2661.
[10] J. Chen, W. Ouyang, W. Yang, J.H. He, X. Fang, Adv. Funct. Mater. (2020) 1909909.
[11] N.N. Wang, L. Cheng, R. Ge, S.T. Zhang, Y.F. Miao, W. Zou, C. Yi, Y. Sun, Y. Cao, R. Yang, Y.Q. Wei, Q. Guo, Y. Ke, M.T. Yu, Y.Z. Jin, Y. Liu, Q.Q. Ding, D.W. Di, L. Yang, G.C. Xing, H. Tian, C.H. Jin, F. Gao, R.H. Friend, J.P. Wang, W. Huang, Nat. Photon. 10 (2016) 699–704.
[12] H.M. Zhu, Y.P. Fu, F. Meng, X.X. Wu, Z.Z. Gong, Q. Ding, M.V. Gustafsson, M. T. Trinh, S. Jin, X.Y. Zhu, Nat. Mater. 14 (2015) 636–642.
[13] J.Z. Song, J.H. Li, X.M. Li, L.M. Xu, Y.H. Dong, H.B. Zeng, Adv. Mater. 27 (2015) 7162–7167.
[14] S. Kumar, J. Jagielski, N. Kallikounis, Y.H. Kim, C. Wolf, F. Jenny, T. Tian, C. J. Hofer, Y.C. Chiu, W.J. Stark, T.W. Lee, C.J. Shih, Nano Lett. 17 (2017) 5277–5284.
[15] P. Liu, X.X. He, J.H. Ren, Q. Liao, J.N. Yao, H.B. Fu, ACS Nano 11 (2017) 5766–5773.
[16] S.W. Eaton, M.L. Lai, N.A. Gibson, A.B. Wong, L.T. Dou, J. Ma, L.W. Wang, S. R. Leone, P.D. Yang, Proc. Natl. Acad. Sci. U.S.A. 113 (2016) 1993–1998.
[17] X.X. Wang, M. Shoaib, X. Wang, X.H. Zhang, M. He, Z.Y. Luo, W.H. Zheng, H.L. Li, T.F. Yang, X.L. Zhu, L.B. Ma, A.L. Pan, ACS Nano 12 (2018) 6170–6178.
[18] I. Dursun, Y.Z. Zheng, T.L. Guo, M. De Bastiani, B. Turedi, L. Sinatra, M.A. Hague, B. Sun, A.A. Zhumekenov, M.I. Saidaminov, F.P.G. de Arquer, E.H. Sargent, T. Wu, Y.N. Gartstein, O.M. Bakr, O.F. Mohammed, A.V. Malko, ACS Energy Lett. 3 (2018) 1492–1498.
[19] A.P. Schlaus, M.S. Spencer, K. Miyata, F. Liu, X.X. Wang, I. Datta, M. Lipson, A. L. Pan, X.Y. Zhu, Nat. Commun. 10 (2019) 265.
[20] Z. Liu, Y. Mi, X. Guan, Z. Su, X. Liu, T. Wu, Adv. Opt. Mater. 6 (2018) 1800413.
[21] A.M. Al-Amri, B. Cheng, J.H. He, IEEE Trans. Nano. 18 (2019) 1–12.
[22] D. Periyanagounder, T.-C. Wei, T.-Y. Li, C.-H. Lin, T.P. Gonçalves, H.-C. Fu, D.-S. Tsai, J.-J. Ke, H.-W. Kuo, K.-W. Huang, N. Lu, X. Fang, J.-H. He, Adv. Mater. 32 (2020) 1904634.
[23] C.H. Lin, B. Cheng, T.Y. Li, J.R.D. Retamal, T.C. Wei, H.C. Fu, X. Fang, J.H. He, ACS Nano 13 (2019) 1168–1176.
[24] Y.H. Kim, G.H. Lee, Y.T. Kim, C. Wolf, H.J. Yun, W. Kwon, C.G. Park, T.W. Lee, Nano Energy 38 (2017) 51–58.
[25] M.-H. Shang, J. Zhang, P. Zhang, Z. Yang, J. Zheng, M.A. Haque, W. Yang, S.-H. Wei, T. Wu, J. Phys. Chem. Lett. 10 (2019) 59–66.
[26] E.B. Bi, H. Chen, F.X. Xie, Y.Z. Wu, W. Chen, Y.J. Su, A. Islam, M. Gratzel, X. D. Yang, L.Y. Han, Nat. Commun. 8 (2017) 15330.
[27] C. Wu, Y.T. Zou, T. Wu, M.Y. Ban, V. Pecunia, Y.J. Han, Q.P. Liu, T. Song, S. Duhm, B.Q. Sun, Adv. Funct. Mater. 27 (2017) 1700338.
[28] B. Cheng, T.-Y. Li, P. Maity, P.-C. Wei, D. Nordlund, K.-T. Ho, D.-H. Lien, C.-H. Lin, R.-Z. Liang, X. Miao, I.A. Ajia, J. Yin, D. Sokaras, A. Javey, I.S. Roqan, O. F. Mohammed, J.-H. He, Commun. Phys. 1 (2018) 80.
[29] Z. Fang, M. Shang, Y. Zheng, T. Zhang, Z. Du, G. Wang, X. Duan, K.-C. Chou, C.-H. Lin, W. Yang, X. Hou, T. Wu, Mater. Horiz. (2020), https://doi.org/10.1039/c9mh01788g.
[30] G. Grancini, C. Roldan-Carmona, I. Zimmermann, E. Mosconi, X. Lee, D. Martineau, S. Narbey, F. Oswald, F. De Angelis, M. Graetzel, M.K. Nazeeruddin, Nat. Commun. 8 (2017) 15684.
[31] H. Cho, Y.H. Kim, C. Wolf, H.D. Lee, T.W. Lee, Adv. Mater. 30 (2018) 1704587.
[32] Y. Wei, Z. Cheng, J. Lin, Chem. Soc. Rev. 48 (2019) 310–350.
[33] Q. Zhang, R. Su, W. Du, X. Liu, L. Zhao, S.T. Ha, Q. Xiong, Small Methods 1 (2017) 1700163.
[34] C.-H. Lin, H.-C. Fu, B. Cheng, M.-L. Tsai, W. Luo, L. Zhou, S.-H. Jang, L. Hu, J.-H. He, npj 2D Mater. Appl 2 (2018) 23.
[35] A. Rubino, M. Anaya, J.F. Galisteo-Lopez, T.C. Rojas, M.E. Calvo, H. Miguez, ACS Appl. Mater. Interfaces 10 (2018) 38334–38340.
[36] L.L. Gu, D.Q. Zhang, M. Kam, Q.P. Zhang, S. Poddar, Y. Fu, X.L. Mo, Z.Y. Fan, Nanoscale 10 (2018) 15164–15172.
[37] Y.X. Chen, Q.Q. Ge, Y. Shi, J. Liu, D.J. Xue, J.Y. Ma, J. Ding, H.J. Yang, J.S. Hu, L. J. Wan, J. Am. Chem. Soc. 138 (2016) 16196–16199.
[38] J. Cao, F. Wang, H. Yu, Y. Zhou, H.P. Lu, N. Zhao, C.P. Wong, J. Mater. Chem. 4 (2016) 10223–10230.
[39] A. Waleed, M.M. Tavakoli, L. Gu, Z. Wang, D. Zhang, A. Manikandan, Q. Zhang, R. Zhang, Y.L. Chueh, Z. Fan, Nano Lett. 17 (2017) 523–530.
[40] A. Waleed, M.M. Tavakoli, L. Gu, S. Hussain, D. Zhang, S. Poddar, Z. Wang, R. Zhang, Z. Fan, Nano Lett. 17 (2017) 4951–4957.
[41] Q. Zhang, D. Zhang, L. Gu, K.H. Tsui, S. Poddar, Y. Fu, L. Shu, Z. Fan, ACS Nano 14 (2020) 1577–1585.
[42] Z. Liu, Y. Li, X. Guan, Y. Mi, A. Al-Hussain, S.T. Ha, M.-H. Chiu, C. Ma, M.R. Amer, L.-J. Li, J. Liu, Q. Xiong, J. Wang, X. Liu, T. Wu, J. Phys. Chem. Lett. 10 (2019) 2363–2371.
[43] G.H. Wei, D.A. Czaplewski, E.J. Lenferink, T.K. Stanev, I.W. Jung, N.P. Stern, Sci. Rep. 7 (2017) 3324.
[44] J. Renard, R. Songmuang, C. Bougerol, B. Daudin, B. Gayral, Nano Lett. 8 (2008) 2092–2096.
[45] T.C. Wei, S. Mokkapati, T.Y. Li, C.H. Lin, G.R. Lin, C. Jagadish, J.H. He, Adv. Funct. Mater. 28 (2018) 1707175.
[46] P. Brenner, M. Stulz, D. Kapp, T. Abzieher, U.W. Paetzold, A. Quintilla, I. A. Howard, H. Kalt, U. Lemmer, Appl. Phys. Lett. 109 (2016) 141106.
[47] X.X. Wang, H. Zhou, S.P. Yuan, W.H. Zheng, Y. Jiang, X.J. Zhuang, H.J. Liu, Q. L. Zhang, X.L. Zhu, X. Wang, A.L. Pan, Nano Res. 10 (2017) 3385–3395.
[48] C. Zhang, W. Li, D. Yu, Y. Wang, M. Yin, H. Wang, Y. Song, X. Zhu, P. Chang, X. Chen, D. Li, Adv. Mater. Interfaces 4 (2017) 1601116.
[49] H.K. Liang, B. Meng, G.Z. Liang, J. Tao, Y.D. Chong, Q.J. Wang, Y. Zhang, Adv. Mater. 25 (2013) 6859–6863.
[50] S. Das, M.J. Hossain, S.-F. Leung, A. Lenox, Y. Jung, K. Davis, J.-H. He, T. Roy, Nano Energy 58 (2019) 47–56.
[51] S. Schonhuber, M. Brandstetter, T. Hisch, C. Deutsch, M. Krall, H. Detz, A. M. Andrews, G. Strasser, S. Rotter, K. Unterrainer, Optica 3 (2016) 1035–1038.
[52] X.M. Li, Y. Wang, H.D. Sun, H.B. Zeng, Adv. Mater. 29 (2017) 1701185.
[53] G. Weng, J. Tian, S. Chen, J. Xue, J. Yan, X. Hu, S. Chen, Z. Zhu, J. Chu, Nanoscale 11 (2019) 10636–10645.
[54] G. Weng, J. Xue, J. Tian, X. Hu, X. Bao, H. Lin, S. Chen, Z. Zhu, J. Chu, ACS Photonics 5 (2018) 2951–2959.
[55] T.S. Kao, Y.H. Chou, C.H. Chou, F.C. Chen, T.C. Lu, Appl. Phys. Lett. 105 (2014) 231108.
[56] C. Li, Z. Zang, C. Han, Z. Hu, X. Tang, J. Du, Y. Leng, K. Sun, Nano Energy 40 (2017) 195–202.
[57] X. Tang, Z. Hu, W. Chen, X. Xing, Z. Zang, W. Hu, J. Qiu, J. Du, Y. Leng, X. Jiang, L. Mai, Nano Energy 28 (2016) 462–468.
[58] T. Fan, J. Lu, Y. Chen, W. Yuan, Y. Huang, J. Mater. Sci. Mater. Electron. 30 (2019) 1084–1088.
[59] F. Zhang, C. Chen, S.V. Kershaw, C. Xiao, J. Han, B. Zou, X. Wu, S. Chang, Y. Dong, A.L. Rogach, H. Zhong, ChemNanoMat 3 (2017) 303–310.
[60] D. Zhang, Y. Yu, Y. Bekenstein, A.B. Wong, A.P. Alivisatos, P. Yang, J. Am. Chem. Soc. 138 (2016) 13155–13158.
[61] S. Seth, A. Samanta, Sci. Rep. 6 (2016) 37693.
[62] Z. Wen, W. Zhai, C. Liu, J. Lin, C. Yu, Y. Huang, J. Zhang, C. Tang, RSC Adv. 9 (2019) 24928–24934.
[63] H. Huang, L. Wu, Y. Wang, A.F. Richter, M. Döblinger, J. Feldmann, Nanomaterials 10 (2020) 72.
[64] M.C. Brennan, S. Draguta, P.V. Kamat, M. Kuno, ACS Energy Lett. 3 (2018) 204–213.
[65] F. Zhu, L. Men, Y. Guo, Q. Zhu, U. Bhattacharjee, P.M. Goodwin, J.W. Petrich, E. A. Smith, J. Vela, ACS Nano 9 (2015) 2948–2959.
[66] N. Zhou, Y. Bekenstein, C.N. Eisler, D. Zhang, A.M. Schwartzberg, P. Yang, A. P. Alivisatos, J.A. Lewis, Sci. Adv. 5 (2019), eaav8141.
[67] G. Xu, Y. Li, J. Yan, X. Lv, Y. Liu, B. Cai, Mater. Res. Lett. 7 (2019) 203–209.
[68] L. Dou, M. Lai, C.S. Kley, Y. Yang, C.G. Bischak, D. Zhang, S.W. Eaton, N. S. Ginsberg, P. Yang, Proc. Natl. Acad. Sci. U.S.A. 114 (2017) 7216–7221.
[69] Y. Li, S. Guan, Y. Liu, G. Xu, B. Cai, Optic Express 26 (2018) 33856–33864.
[70] C.H. Lin, C.Y. Kang, T.Z. Wu, C.L. Tsai, C.W. Sher, X. Guan, P.T. Lee, T. Wu, C. H. Ho, H.C. Kuo, J.H. He, Adv. Funct. Mater. (2020) 1909275.

[71] Z.N. Song, A. Abate, S.C. Watthage, G.K. Liyanage, A.B. Phillips, U. Steiner, M. Graetzel, M.J. Heben, Adv. Energy Mater. 6 (2016) 1600846.
[72] M.A. Haque, A. Syed, F.H. Akhtar, R. Shevate, S. Singh, K.-V. Peinemann, D. Baran, T. Wu, ACS Appl. Mater. Interfaces 11 (2019) 29821–29829.
[73] P.S. Whitfield, N. Herron, W.E. Guise, K. Page, Y.Q. Cheng, I. Milas, M.K. Crawford, Sci. Rep. 6 (2016) 35685.

Dr. Chun-Ho Lin is currently a postdoctoral fellow in University of New South Wales (UNSW). He received his Ph.D. degree in Electrical Engineering from King Abdullah University of Science and Technology (KAUST) in 2019 and M.S. degree in Optoelectronics and Photonics Engineering from National Taiwan University in 2014. His research focuses on the development of halide perovskite-based optoelectronics using novel device design and contact engineering. His research activities also include lithography patterning of hybrid perovskites, highly stable perovskite quantum dot papers, and flexible electronics.

Mr. Ting-You Li received the B.S. Degree (with the honor of the top-rated prize) in applied chemical engineering from National Taipei University of Technology, Taiwan, in 2014, and the M.S. degree in electrical engineering from KAUST in 2017. His main areas of research interest are the synthesis of organic-inorganic halide perovskite, two-dimensional perovskite optoelectronic device, and their fundamental physical properties.

Mr. Jing Zhang is currently pursuing his M.S under the supervision of Prof. Jing Liu at School of Precision Instruments and Optoelectronics Engineering, Tianjin University, China. His research focuses on fabrication and characterization of photoelectric sensors and memory device based on 2D materials. His research interest also includes energy harvesting and exploration of physical properties of novel (nano) materials.

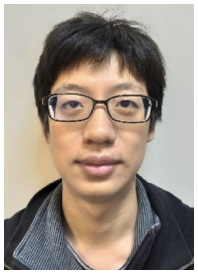

Zong-Yi Chiao is a master student in the Department of Physics at National Taiwan University under supervision of Prof. Yu-Jung Lu. He received his B.S. degree in Physics from National Central University in 2016. His current research interests focus on investigating the optical properties of advanced materials and their applications.

Dr. Pai-Chun Wei is a research scientist affiliated to King Abdullah University of Science and Technology (KAUST). He received B.S. (2002), M.S. (2004), and Ph.D (2009) degrees from the Department of Materials Science and Engineering at National Tsing Hua University (Taiwan) and started his academic carrier at the institute of physics, Academia Sinica (Taiwan) in 2011. His research interests include molecular beam epitaxy of III–V semiconductors, single-crystal growth, lattice dynamics of low-thermal-conductivity materials, and thermoelectric materials.

Dr. Hui-Chun Fu received her Ph.D. degree in Electrical Engineering from King Abdullah University of Science and Technology (KAUST) with Prof. Jr-Hau He in 2019. She is currently carrying out her postdoctoral research with Prof. Song Jin at Chemistry, Wisconsin University. Her research focuses on the development of integrated photoelectrochemical system for simultaneous conversion and storage of intermittent solar energy. She made progress on the development of solar cells and photoelectrodes for electrocatalysis, solar energy conversion and storage including solar water splitting, solar to CO_2 reduction and solar redox flow batteries.

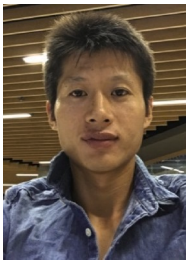

Dr. Long Hu is a research associate in the School of materials Science and Engineering, UNSW Sydney (Australia) under the supervision of Prof. Shujuan Huang and Prof. Tom Wu. He received his PH.D. degree from Huazhong University of Science and Technology at 2016. His current research interest is on high performance optoelectronic devices such as photovoltaic cell and phototransistor based on colloidal quantum dots and halide perovskite.

Meng-Ju Yu is currently a research assistant in the Research Center for Applied Sciences at Academia Sinica under supervision of Prof. Yu-Jung Lu. He received his B.S. degree from the National University of Kaohsiung and M.S. degree from the National Chiao Tung University, Taiwan in 2017. His research interests mainly focus on investigating strong light-matter interactions in the nanoscale resonant structures to enhance the performance of optoelectronic devices.

Dr. Ghada H. Ahmed obtained her Ph.D. degree in Chemistry at King Abdullah University of Science and Technology (KAUST), Saudi Arabia under the supervision of prof. Omar F. Mohammed. Before joining KAUST, she received her M.Sc. degree in Nanoscience and Technology at Nile University (NU), Cairo, Egypt. Her research interest focuses on the photophysical aspects of novel nanoscale materials and their uses in nascent solar and light-harvesting technologies.

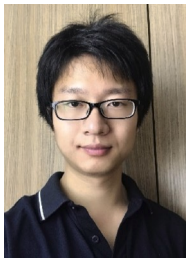

Xinwei Guan is currently a PhD student in the department of Materials Science & Engineering, UNSW (Australia). He received his MS degree from KAUST (Saudi Arabia) and bachelor's degree from Huazhong University of Science & Technology (China). His current research interests include hybrid perovskites, non-volatile memory devices, and optoelectronic devices.

Dr. Chih-Hsiang Ho currently is the Founder of Raysolution LLC in San Jose, CA. He received Ph.D. degree from the Electrical and Computer Engineering of Purdue University in 2014. He was with AU Optronics, Hsinchu, Taiwan, where he was involved in research with LCD panel design. His primary research interests include low-power and variation-tolerant circuit design and modeling of advanced device and circuit reliability.

Dr. Tom Wu received his B.S. from Zhejiang University and Ph.D. from the University of Maryland, College Park in 2002. Before joining University of New South Wales (UNSW) in Sydney as a full professor, he worked as postdoc in Argonne National Laboratory in Chicago, assistant professor in Nanyang Technological University (NTU) Singapore, and associate professor in King Abdullah University of Science and Technology (KAUST). His group works in the areas of oxide thin films, nanomaterials, and hybrid perovskites, with a focus on their electronic, magnetic and optical functionalities.

Dr. Boon S. Ooi is a Professor of Electrical Engineering at KAUST. He received his Ph.D. degree from the University of Glasgow, United Kingdom, in 1994. His research includes the study of III-Nitride based materials and optoelectronic devices, and visible light communication (LiFi) and underwater optical communications. He has served on the technical program committee of CLEO, PW, IPC, ISLC and IEDM. He is the associate editor of Optics Express and IEEE Photonics Journal. He is an elected Fellow of the United States National Academy of Inventors (NAI), and a Fellow of OSA, SPIE and IoP (UK).

Prof. Omar F. Mohammed specialises in fundamental understanding of carrier dynamics in a variety of solar cell systems, including semiconductor quantum dots, polymers and perovskite solar cells with the aid of cutting-edge nanotechnology, ultrafast laser spectroscopy and four-dimensional electron imaging. He is working as Associate Professor in Department of Chemical Science, King Abdullah University of Science and Technology, Saudi Arabia.

Dr. Yu-Jung Lu is an Assistant Research Fellow of Research Center for Applied Sciences at Academia Sinica and an Assistant Professor of Department of Physics at National Taiwan University. Dr. Lu received her Ph.D. in Physics from National Tsing Hua University in 2013. She worked at California Institute of Technology (Caltech) as a postdoc from 2015 to 2017. She is a material physicist, her research interests are within an interdisciplinary field of active plasmonics/optoelectronics with a particular focus on semiconductor nanostructure devices to investigate harvesting, generating, and manipulating light at the nanoscale.

Dr. Xiaosheng Fang is professor in Department of Materials Science at Fudan University, China. He received his Ph.D. degree from the Institute of Solid State Physics (ISSP), Chinese Academy of Sciences in 2006. After then, he was a JSPS postdoctoral fellow at the National Institute for Materials Science, Japan, as well as a research scientist at the International Center for Young Scientists (ICYS). He was a visiting scholar at MIT and Harvard University in 2009 and 2016, respectively. His current research topic mainly focuses on inorganic semiconductors and high-performance photodetectors.

Dr. Jr-Hau He is a Professor in Department of Materials Science and Engineering at City University of Hong Kong. He has been a pioneer in optoelectronics, which reflects on his achievement of photon management on the light harvesting devices. He has conducted highly interdisciplinary researches to bridge those gaps between various research fields and between academia and industry. He is a Fellow of OSA, RSC and SPIE, and a senior member of IEEE. Visit his web for more information (personal.cityu.edu.hk/jrhauhe).